

Pd(II)-immobilized on a nanoporous triazine-based covalent imine framework for facile cyanation of haloarenes with $K_4Fe(CN)_6$

Pillaiyar Puthiaraj, Kwangsun Yu, Sang Eun Shim, Wha-Seung Ahn*

Department of Chemistry and Chemical Engineering, Inha University, Incheon 402-751, South Korea

ARTICLE INFO

Keywords:

Covalent organic frameworks
Schiff-base networks
Palladium
Cyanation
Potassium ferrocyanide

ABSTRACT

A porous covalent organic framework incorporated with both imine and triazine functionalities (TPA-TCIF) was synthesized by Schiff-base condensation of 2,4,6-tris(4-aminophenyl)triazine and tris(4-formylphenyl)amine under the solvothermal condition of a 1-butanol:1,2-dichlorobenzene mixture. The resulting TPA-TCIF was a highly ordered crystalline network with surface area of $2938 \text{ m}^2 \text{ g}^{-1}$, which was among the highest reported imine-based porous covalent organic frameworks. TPA-TCIF was also stable in water and other organic solvents. Pd(II) was immobilized into TPA-TCIF network and the resultant Pd/TPA-TCIF was tested as a catalyst for the additive-free cyanation of haloarenes with non-toxic $K_4[Fe(CN)_6]$. The catalyst showed excellent catalytic activity, and both electron-donating / -withdrawing groups attached to the *para*- and *meta*-positions of bromoarenes produced the respective nitriles with good to excellent yields. The catalyst could be reused up to five times without noticeable loss of activity or catalyst poisoning by cyanide ions during the reaction.

1. Introduction

Covalent organic frameworks (COFs) are composed of organic building blocks having light-weight elements (C, B, O, N, and Si) interconnected through strong covalent bonding. The COFs have unique features of low skeleton density, permanent porosity with large surface area, structural diversity originating from the selection of synthesis precursors, surface hydrophobicity, and high chemical stability [1–3]. These interesting features make them useful in various applications: catalysis [4,5], gas storage [6], sensors [7,8], optoelectronics [9], and drug delivery [2]. COFs can be prepared by various organic reactions such as Schiff-base formation [3,10,11], trimerization of nitriles [12], boronate-ester formation [13], nucleophilic reaction [14,15], coupling reaction [16], Friedel-Crafts reactions [17,18], and others [19–21]. Among these, Schiff-base chemistry creating the imine (C=N) linkage is attracting increased attention owing to the simple condensation of aldehydes and amines without the addition of any metal catalyst and the formation of a structure containing π -conjugated free lone-pair electrons.

Taking advantages of the free lone-pair electrons, some imine-based COFs have been used as catalyst supports to anchor Pd(II) ions for various organic transformations [22–26]. Thus, Ding et al. prepared Pd/COF-LZU1 with surface area of $146 \text{ m}^2 \text{ g}^{-1}$ and used it for Suzuki coupling reaction [22]. Zhang et al. prepared a Pd(II)-grafted triazine-

based COF-SDU-1 with surface area of $1052 \text{ m}^2 \text{ g}^{-1}$ for a coupling reaction of silanes and iodoarenes [23]. Esteves et al. reported Pd(OAc)₂@COF-300 with surface area of $270 \text{ m}^2 \text{ g}^{-1}$ for Suzuki-, Heck-, and Sonogashira coupling reactions [24]. Bimetallic Rh(I)/Pd(II)-incorporated imine-based COF with surface area of $847 \text{ m}^2 \text{ g}^{-1}$ was also reported for the one-pot addition-oxidation tandem reaction [25]. Gao et al. reported a bimetallic Mn/Pd-incorporated imine-based COF for the Heck-epoxidation tandem reaction [26]. Similarly, Cu, Ag, and Ir ions could also be immobilized on imine-based COFs as catalysts for other organic reactions [3,10,27–30]. Most of the above-mentioned COF supported materials, however, were amorphous and suffered from low stability under the reaction conditions [10,22,24,27–29]. In comparison, porous crystalline frameworks with a higher density of lone-pair electrons would be more appropriate for immobilization of transition metal ions and promoting the diffusion of reactants, in order to augment the catalytic activity and improve the reusability [30].

Nitriles are a valuable class of building blocks in pharmaceuticals, dyes, agrochemicals, and other organic products [31,32]. Traditional routes for the synthesis of nitriles have been Rosenmund-von Braun reaction [33] and Sandmeyer reaction [34] at a temperature $> 150 \text{ }^\circ\text{C}$ with stoichiometric amount of CuCN. Recently, Cu- and Ni-catalyzed cyanations have also been employed with a variety of cyanide sources (NaCN [31], KCN [35], HCN [36], Zn(CN)₂ [37], CuSCN [38], and (CH₃)₃SiCN [39]). Nevertheless, toxic and expensive cyanide source

* Corresponding author.

E-mail address: whasahn@inha.ac.kr (W.-S. Ahn).

and high temperature were required. To overcome these problems, Beller et al. proposed a Pd-catalyzed cyanation with low-cost cyanide source of $K_4[Fe(CN)_6]$ [40,41]. A number of homogeneous Pd-complex catalysts were tested for this reaction, but they required expensive ligands and suffered from the problems of non-reusability, tedious workup, and metal contamination in the product [42–45]. To avoid these difficulties, heterogeneous Pd-catalysts such as NHC-Pd polymer [46], Pd@CuFe₂O₄ [47], IL@SBA-15-Pd [48], Pd-LHMS-3 [49], Pd/silica [50,51] and Pd/C [52] were also reported recently for the cyanation of haloarenes. However, often the active Pd metal species were leached out of the catalyst, or severe agglomeration of Pd nanoparticles in successive runs was observed, which limited the scope of the applicable substrates [46–48,50–52]. Therefore, the synthesis of a functional crystalline carrier with high stability for supporting Pd(II) ions is strongly desired for this reaction.

In this work, a robust crystalline COF containing imine and triazine functionalities with desirable textural properties was synthesized via a solvothermal reaction between 2,4,6-tris(4-aminophenyl)triazine (TAPT) and tris(4-formylphenyl)amine (TFPA). After establishing its high stability in various solvents, it was utilized as a carrier for anchoring Pd(OAc)₂. The catalytic performance of the Pd(II)-immobilized COF was examined systematically in the cyanation of haloarenes, demonstrating excellent activity and recyclability.

2. Experimental section

2.1. Materials

4-aminobenzonitrile, triflic acid, TFPA, 1,2-dichlorobenzene, 1-butanol, acetic acid, anhydrous N,N'-dimethylformamide (DMF), $K_4[Fe(CN)_6] \cdot 3H_2O$, Pd(OAc)₂, ethanol, methanol, and 1,2-dichloromethane were obtained from Sigma-Aldrich (USA). All other chemicals and solvents used in this study were collected from TCI (Japan) and Merck (Korea), and all were used without further purification. TAPT was prepared according to the published procedure [53], and the product was confirmed by nuclear magnetic resonance (NMR) spectroscopy (Fig. S1–S2).

2.2. Synthesis of TPA-TCIF

TFPA (1 mmol; 329 mg), TAPT (1 mmol; 354 mg), 3 M acetic acid (1 mL), 1-butanol (6 mL), and 1,2-dichlorobenzene (2 mL) were charged into a 15-mL ACE pressure tube and sealed off, and then heated at 120 °C. After 72 h, the solid product was collected by filtration and washed several times with DMF and ethanol. Finally, the obtained product was dried at 200 °C for 10 h under high vacuum condition. The product of porous covalent imine framework incorporated with both triphenylamine and triazine functionalities was designated as TPA-TCIF.

2.3. Synthesis of Pd/TPA-TCIF

The Pd/TPA-TCIF catalyst was synthesized via impregnation of Pd(OAc)₂ into TPA-TCIF. In a typical procedure, Pd(OAc)₂ (30 mg) was dispersed in dichloromethane (30 mL). After adding TPA-TCIF (500 mg) to the solution, the mixture was refluxed with stirring for 3 h. The Pd(II) bound TPA-TCIF was collected by filtration and washed with dichloromethane and acetone to remove the excess Pd(OAc)₂. Finally, the product was dried at 60 °C in a vacuum for 1 h.

2.4. Characterization of the COF host and the catalyst prepared

Fourier transform-infrared spectra were obtained from a Bruker VERTEX 80 V spectrometer. Solid-state ¹³C cross polarization-magic angle spinning NMR and liquid-state ¹H and ¹³C NMR were measured on a Bruker Avance III 400 MHz spectrometer. X-ray photoelectron

spectra (XPS) were obtained from a hemispherical analyzer (Thermo Scientific, USA). Elemental analysis was done on a Thermo EA1112 (USA). Powder X-ray diffraction (XRD) were conducted using a Rigaku (DMAX-2500) diffractometer using Cu K α radiation ($\lambda = 1.5418\text{\AA}$). The nitrogen sorption experiment was conducted at 77 K using a BELsorp-max analyzer (BEL, Japan). Before the analysis, the materials were treated at 200 °C under high vacuum for 12 h. Field emission scanning electron microscope (FESEM) and field emission transmission electron microscope (FETEM) with energy-dispersive X-ray spectrometry (EDS) images were taken on a Hitachi S-4300 and a JEM-2100 F (JEOL), respectively. The palladium content on the support was determined by inductively coupled plasma-optical emission spectrometry (ICP-OES; PerkinElmer Optima 7300DV, USA).

2.5. Catalytic cyanation of haloarenes

Haloarene (1 mmol), Na₂CO₃ (1 mmol), $K_4[Fe(CN)_6]$ (0.2 mmol), Pd/TPA-TCIF (40 mg), and DMF (4 mL) were charged into a 15-mL ACE pressure tube and capped, and then heated at 110 °C with constant stirring. After 20 h, the catalyst was isolated by centrifugation and washed with ethyl acetate and water. The filtered organic phase was collected and the conversion of haloarene was measured using an Agilent HP6890 model gas chromatography (GC) furnished with a flame ionization detector and an HP-5 capillary column. Subsequently, the organic phase was concentrated, and then the nitrile product was purified using a silica gel column chromatography.

3. Results and discussion

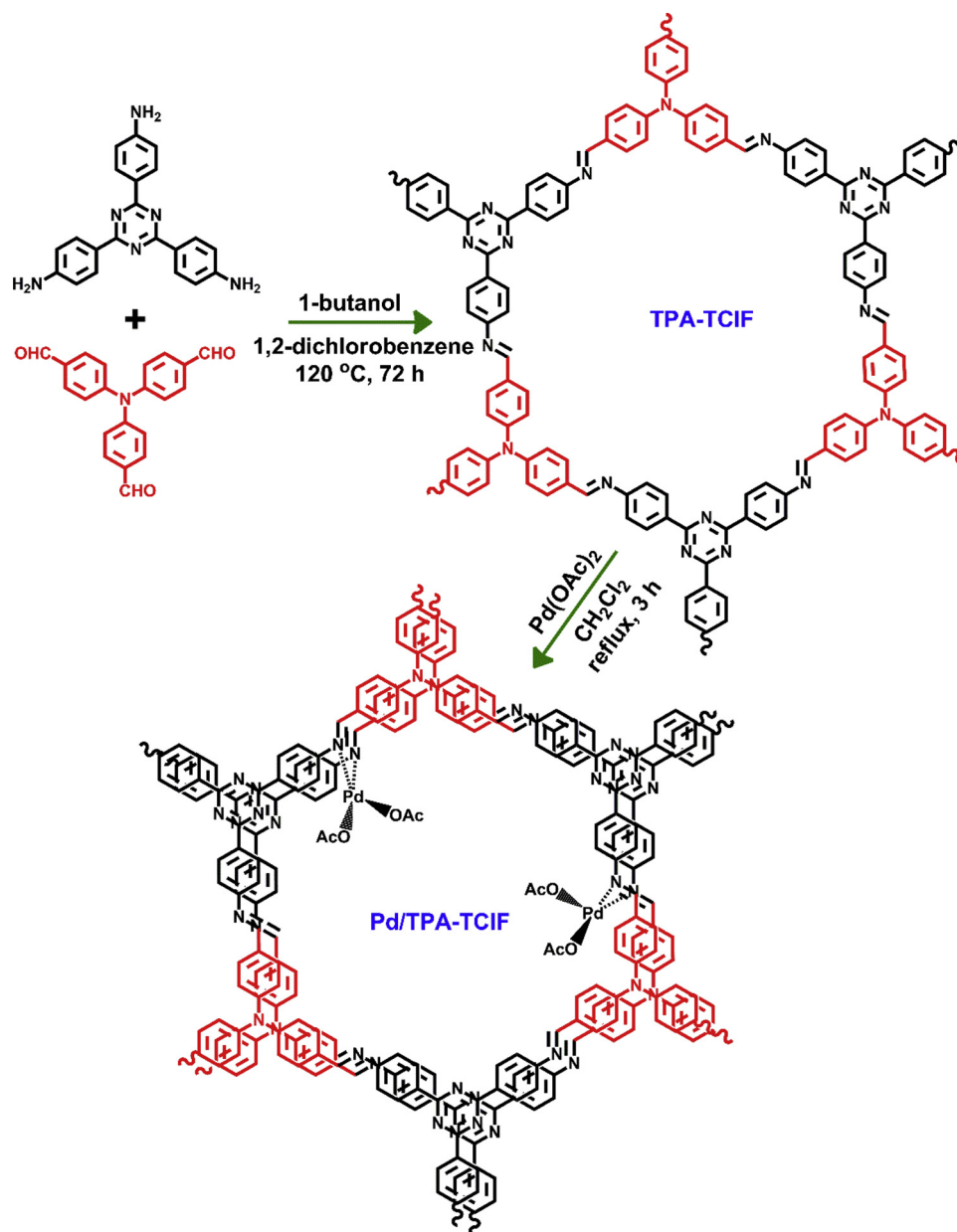
3.1. Catalyst characterization

The covalent imine framework containing both triphenylamine and triazine units (TPA-TCIF) was synthesized by the Schiff-base reaction between TFPA and TAPT as described in Scheme 1. The reaction was conducted in the presence of 3 M acetic acid using a mixture of 1-butanol/1,2-dichlorobenzene solvent mixture (3:1 by volume) at 120 °C for 72 h. The synthesized material was insoluble and highly stable in both water and organic solvents such as toluene, acetone, tetrahydrofuran, chloroform, DMF, DMSO, and acetonitrile (Fig. S3). The successful growth of the TPA-TCIF network was confirmed using infrared spectroscopy, elemental analysis, solid-state NMR, powder XRD, N₂ sorption isotherm, XPS, and electron microscope techniques.

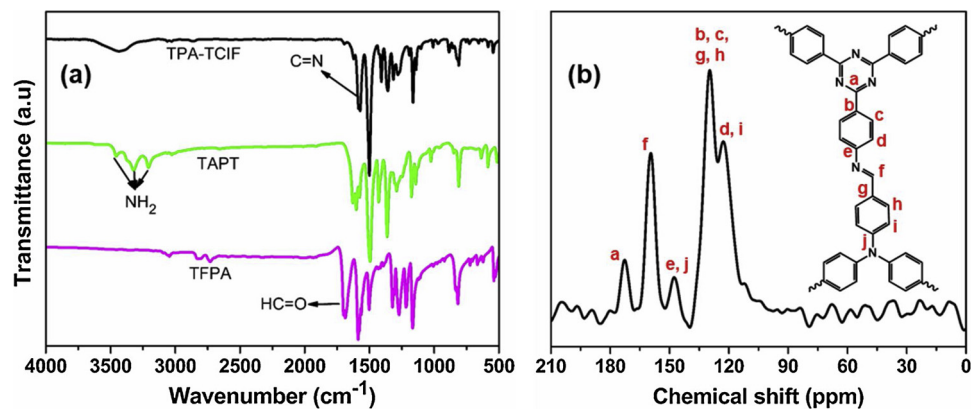
The infrared spectra of TPA-TCIF in Fig. 1(a), the C=O (1689 cm⁻¹) and -NH₂ (3208, 3325, and 3464 cm⁻¹) stretching bands completely disappeared and a new characteristic strong stretching peak at 1578 cm⁻¹ was present, indicating the formation of imine bond via Schiff-base reaction of TFPA and TAPT. These two precursors were fully consumed. According to the elemental analysis results, the experimental values of C (79.77%), H (4.19%), and N (15.13%) in the TPA-TCIF sample matched well to the theoretical contents of C (80.11%), H (4.32%), and N (15.57%) with a maximum deviation of ~1% for carbon.

In solid-state NMR (Fig. 1(b)), it displayed a characteristic peak at 159.2 ppm, which was assignable to imine carbons. The other peaks at 173.0, 147.5, and ~128 ppm were assignable to the carbons in triazine, nitrogen attached phenyl groups, and carbons from phenyl, respectively [3]. The deconvoluted C 1s XPS (Fig. 2(a)) revealed five peaks at 284.2, 285.8, 287.8, 288.9, and 291.2 eV, ascribed to the aromatic C=C, C=N, C-N, triazine carbon, and π - π^* transition, respectively [54,55]. The N 1s spectrum (Fig. 2(b)) displayed three deconvoluted peaks at 397.8, 399.0, and 400.7 eV, which can be ascribed to the nitrogen in triazine, imine, and triphenylamine groups, respectively [55,56]. These NMR and XPS results also clearly indicated the formation of the imine bond and the presence of triphenylamine and triazine moieties in the TPA-TCIF network.

The porosity of the synthesized TPA-TCIF material was inspected by



Scheme 1. Synthesis of TPA-TCIF and subsequent Pd(II) immobilization.

Fig. 1. (a) Infrared spectra of TFA, TAPT, and TPA-TCIF and (b) Solid-state ¹³C NMR of TPA-TCIF.

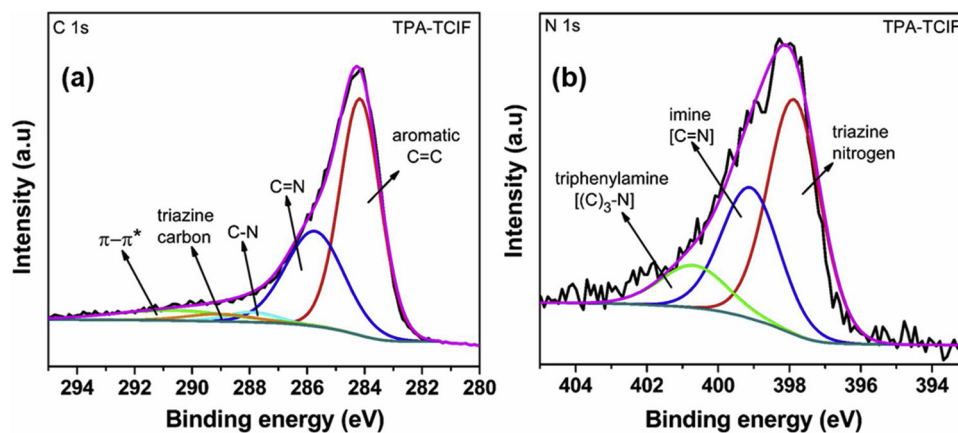


Fig. 2. XPS of (a) C 1s and (b) N 1s core level in TPA-TCIF.

Table 1

Textural properties of the synthesized Schiff-base COF materials.

Frameworks	S_{ABET} ($\text{m}^2 \text{g}^{-1}$)	$V_{0.1}$ ($\text{cm}^3 \text{g}^{-1}$)	V_{tot} ($\text{cm}^3 \text{g}^{-1}$)	$V_{0.1}/V_{\text{tot}}$ (%)	Pore width (nm)
TPA-TCIF	2938	1.09	1.32	82.6	1.5, 1.7
Fresh Pd/TPA-TCIF	2647	0.95	1.21	78.5	1.5, 1.7
Reused Pd/TPA-TCIF	2629	0.93	1.18	78.8	1.5, 1.7

S_{ABET} = BET surface area; $V_{0.1}$ = pore volume at 0.10 bar; V_{tot} = pore volume at 0.99 bar.

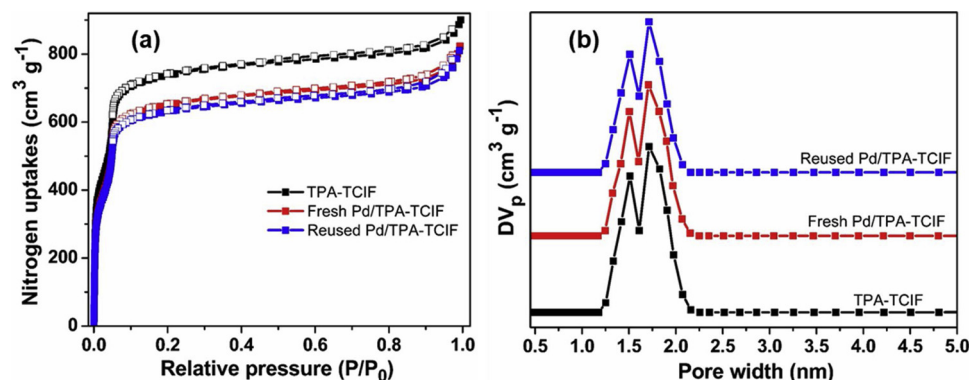


Fig. 3. (a) N_2 sorption isotherms and (b) pore size distributions of TPA-TCIF and fresh/reused Pd/TPA-TCIF catalyst.

N_2 sorption isotherms at 77 K (Table 1). As illustrated in Fig. 3(a), TPA-TCIF showed a type I isotherm with a steep N_2 uptake at < 0.03 bar pressure, implying the existence of micropores in the networks. There was also a secondary sharp increase at ~ 0.08 bar corresponding to another type of uniform pores close to ca. 2 nm in size [57]. Practically no hysteresis was observed here, and the increase in the adsorbed volume at pressure > 0.9 bar is due to N_2 condensation in the inter-particle voids [19]. The levels of microporosity in the TPA-TCIF was 79.6%, as estimated by the ratio of micropore volume to total pore volume [58]. The Brunauer-Emmett-Teller (BET) surface area of TPA-TCIF was $2938 \text{ m}^2 \text{g}^{-1}$ and pore volume of $1.32 \text{ cm}^3 \text{g}^{-1}$, which was among the highest reported recently for imine-based porous COFs [2,3,59–68], and it is close to the TpBD-Me₂ ($3109 \text{ m}^2 \text{g}^{-1}$) and TpAzo ($3038 \text{ m}^2 \text{g}^{-1}$) networks [69]. Fig. 3(b) shows the pore size of the frameworks estimated by non-local density functional theory with slit pore geometry. TPA-TCIF was mainly microporous with uniform pores of 1.5 and 1.7 nm in size.

The powder X-ray diffraction (Fig. 4) of TPA-TCIF displayed a strong intense peak at 4.44° and additional weak peaks at 7.66 , 8.88 , 11.74 , and 22.54° , which corresponded to (100), (210), (200), (310), and (001) reflections of hexagonal 2D honeycomb-type framework, respectively [68], with unit cell parameters $a = b = 19.90 \text{ \AA}$ and

$c = 3.94 \text{ \AA}$. The broad peak of (001) plane is due to the π - π stacking between the framework layers [62]. The d -spacings between the planes were calculated from the powder XRD pattern (Fig. 4) using the Bragg equation (1).

$$n\lambda = 2d \sin\theta \quad (1)$$

where, $\lambda = 1.5418 \text{ \AA}$, $n = \text{integer}$ (here $n = 1$). The d_{100} , d_{210} , d_{200} , d_{310} , and d_{001} values for TPA-TCIF were estimated to be 19.90, 11.54, 9.96, 7.54, and 3.94 \AA , respectively.

The morphology of the synthesized TPA-TCIF was examined using electron microscope techniques. FESEM image of TPA-TCIF (Fig. 5(a)) displayed a cauliflower-like morphology. FETEM image of TPA-TCIF (Fig. 5(b)) showed a parallel aligned planar plate-like structure with a uniform pore diameter.

The highly crystalline TPA-TCIF with a large surface area and high nitrogen content was tested as support to stabilize a Pd salt for the catalytic application. Pd/TPA-TCIF was prepared by treatment of Pd (OAc)₂ with TPA-TCIF in dichloromethane under reflux condition with constant stirring for 3 h (Scheme 1). The powder XRD of Pd/TPA-TCIF (Fig. 4) displayed the same peaks as TPA-TCIF, indicating that the TPA-TCIF framework remained intact after the impregnation. The Pd 3d XPS results of Pd/TPA-TCIF catalyst showed two de-convoluted peaks

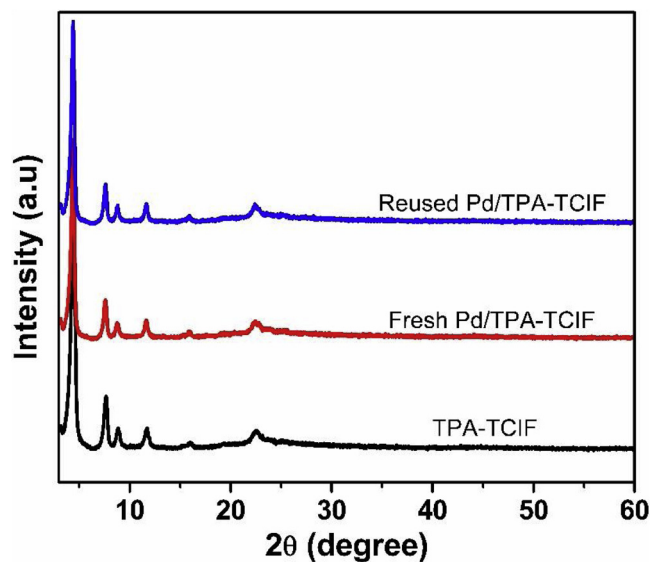


Fig. 4. Powder X-ray diffraction patterns of TPA-TCIF and Pd/TPA-TCIF catalyst (fresh and reused).

centered at 336.8 and 341.9 eV, which were assigned to the Pd 3d_{5/2} and Pd 3d_{3/2} levels, respectively (Fig. 6(a)) [70]. In addition, the peak of imine bond N 1s peak was shifted from 399.0 to 399.7 eV after incorporation of Pd(OAc)₂ (Fig. 6(b)), which is probably due to the interaction between the support nitrogen atom and the palladium salt.

FETEM image of Pd/TPA-TCIF (Fig. 5(c)) did not show any Pd(0) nanoparticles formation, but the FETEM elemental mapping (Fig. 5(d)) showed the presence of C, N, and Pd species with uniform dispersion, which indicate that the Pd²⁺ ions were successfully grafted on the TPA-TCIF support. The surface area (2647 m² g⁻¹) of the Pd/TPA-TCIF catalyst decreased a little compared to those of the pristine support material, caused by the partial filling of Pd(OAc)₂. The palladium loading on TPA-TCIF was estimated to be 1.16 wt% by ICP-OES.

3.2. Cyanation of haloarenes over Pd/TPA-TCIF

The prepared Pd/TPA-TCIF was then explored as a heterogeneous catalyst for the cyanation of haloarenes. Iodoarene has been widely reported as a substrate for the homogeneous palladium-catalyzed cyanation reactions. However, it is not practical for industrialization due to the need for expensive ligands, difficult product separation from the reaction mixture, non-reusability, and the higher price of iodoarene than bromo-/chloro-arenes [42,45]. Therefore, a reusable Pd-catalyst for the cyanation reaction of low-cost bromoarene substrates will be preferable. With these in mind, 4-bromoanisole and K₄[Fe(CN)₆] were used as the model substrate and the cyanating agent, respectively, for the cyanation reaction (Table 2). A series of the experiments were conducted to locate the optimum reaction conditions that maximize the yield of nitrile products. No product was detected in the presence of TPA-TCIF support alone (40 mg) and K₂CO₃ (1 mmol) as a base in DMF at 110 °C (Table 2, entry 1). The homogeneous Pd(OAc)₂ gave only a 22% yield of 4-methoxybenzoxynitrile product (Table 2, entry 2). In contrast, Pd/TPA-TCIF catalyst gave 79% yield of nitrile product

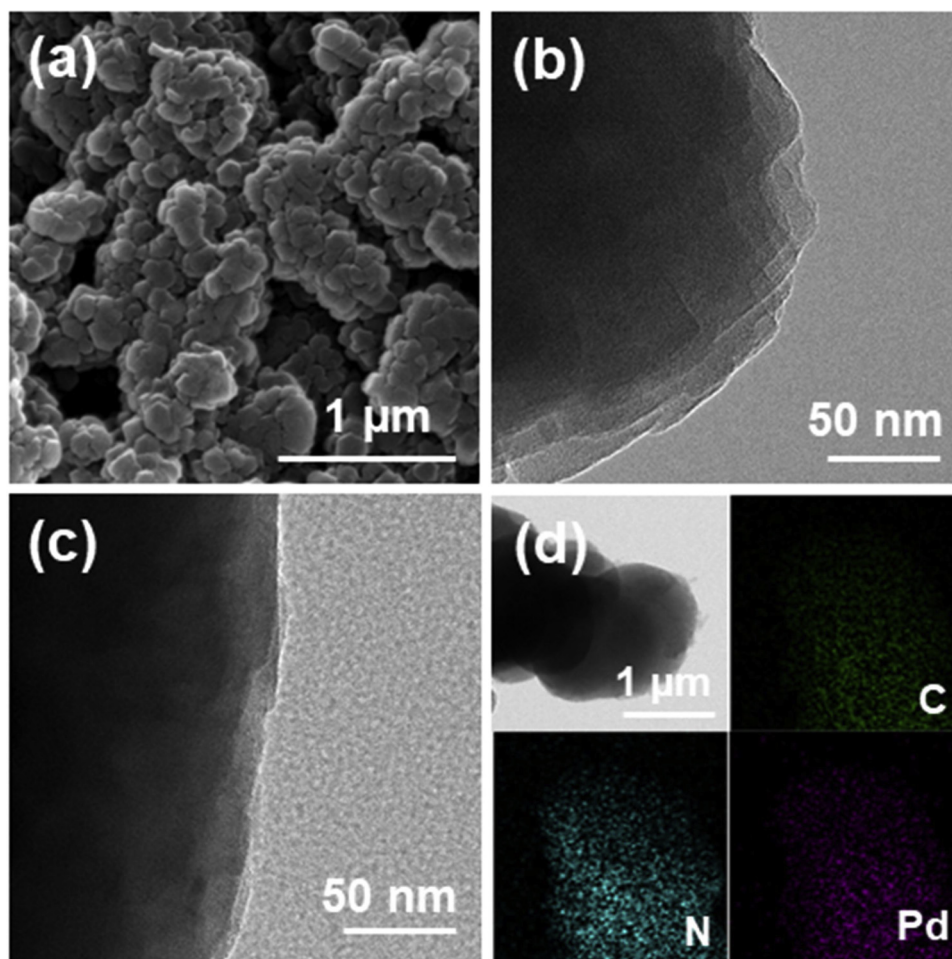


Fig. 5. (a) FESEM and (b) FETEM images of TPA-TCIF, (c) FETEM image of Pd/TPA-TCIF and (d) EDS mapping images for C, N, and Pd elements of Pd/TPA-TCIF.

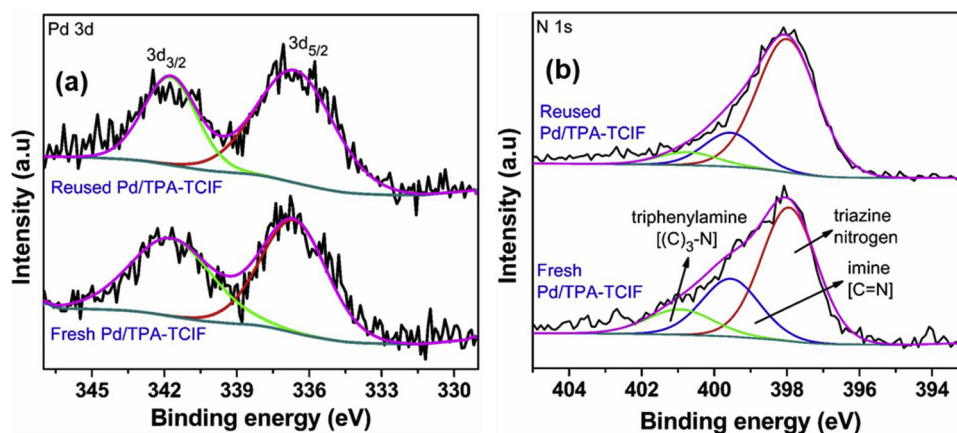


Fig. 6. (a) Pd 3d and (b) N 1s XPS of Pd/TPA-TCIF.

Table 2
Studies of reaction conditions in the cyanation of 4-bromoanisole.^a

Entry	Catalyst	Base	Solvent	GC yield (%)
1	TPA-TCIF	K ₂ CO ₃	DMF	Nil
2 ^b	Pd(OAc) ₂	K ₂ CO ₃	DMF	22
3	Pd/TPA-TCIF	K ₂ CO ₃	DMF	79
4 ^c	Pd(OAc) ₂ /TPA-TCIF	K ₂ CO ₃	DMF	61
5	Pd/TPA-TCIF	K ₂ CO ₃	1,4-Dioxane	Trace
6	Pd/TPA-TCIF	K ₂ CO ₃	^t BuOH	6
7	Pd/TPA-TCIF	K ₂ CO ₃	MeCN	Trace
8	Pd/TPA-TCIF	K ₂ CO ₃	DMSO	62
9	Pd/TPA-TCIF	K ₂ CO ₃	Water	Nil
10	Pd/TPA-TCIF	K ₂ CO ₃	DMF:water	28
11	Pd/TPA-TCIF	K ₂ CO ₃	Toluene	Nil
12	Pd/TPA-TCIF	–	DMF	7
13	Pd/TPA-TCIF	Na ₂ CO ₃	DMF	98
14	Pd/TPA-TCIF	K ₃ PO ₄	DMF	30
15	Pd/TPA-TCIF	NaOAc	DMF	67
16	Pd/TPA-TCIF	TEA	DMF	12
17	Pd/TPA-TCIF	DBU	DMF	14
18 ^d	Pd/TPA-TCIF	Na ₂ CO ₃	DMF	60
19 ^e	Pd/TPA-TCIF	Na ₂ CO ₃	DMF	74
20 ^f	Pd/TPA-TCIF	Na ₂ CO ₃	DMF	Nil
21 ^g	Pd/TPA-TCIF	Na ₂ CO ₃	DMF	77
22 ^h	Pd/TPA-TCIF	Na ₂ CO ₃	DMF	53

^a Reaction conditions: 4-bromoanisole (1 mmol), Pd/TPA-TCIF (40 mg), base (1 mmol), K₄[Fe(CN)₆] (0.2 mmol), solvent (4 mL) 110 °C, 20 h.

^b Pd(OAc)₂ (1 mg; 0.0045 mmol Pd).

^c TPA-TCIF (40 mg), Pd(OAc)₂ (1 mg).

^d Na₂CO₃ (0.5 mmol).

^e 100 °C.

^f 80 °C.

^g Pd/TPA-TCIF (30 mg).

^h Pd/TPA-TCIF (20 mg).

(Table 2, entry 3), suggesting that the Pd anchored on TPA-TCIF is the catalytic active species in the present cyanation reaction. When the reaction was conducted with a mixture of Pd(OAc)₂ and TPA-TCIF instead of Pd/TPA-TCIF, a 61% yield of nitrile product was detected (Table 2, entry 4).

Among the various polar (1,4-dioxane, ^tBuOH, MeCN, DMSO, DMF, water, and DMF-water) and non-polar (toluene) solvents tested (Table 2, entries 3, 5–11), cyanation proceeded well only in DMF. In the absence of any base, a very low 4-bromoanisole conversion (7%) was detected (Table 2, entry 12) because the base is crucial in the dehalogenation step [36,71]. Na₂CO₃ was better than another inorganic

(K₂CO₃, K₃PO₄, and NaOAc) or organic (TEA, and DBU) bases (Table 2, entries 3, 13–17). The product yield decreased to 60% as the Na₂CO₃ amount was reduced to 0.5 mmol (Table 2, entry 18). The reaction temperature and catalyst loading also strongly influenced the cyanation reaction. When the temperature dropped from 110 to 100 °C, the product yield was also decreased from 98% to 74% (Table 2, entry 19) and further decreasing the temperature to 80 °C led to no cyanation product (Table 2, entry 20), implying that the release of cyanide ion from K₄[Fe(CN)₆] is difficult at low temperatures. K₄[Fe(CN)₆] shows low solubility in organic solvents and therefore high energy is required to dissociate the ferrocyanide anion [32,72]. Similarly, when the catalyst loading was decreased from 40 to 30 and 20 mg, the product yield decreased from 98% to 77% and 53% (Table 2, entries 21–22). The kinetics profile (Fig. 7(a)) revealed that the product yield gradually increased and reached a maximum after 20 h. From these screening experiments, the optimal condition for the cyanation of 4-bromoanisole (1 mmol) was established to be Pd/TPA-TCIF catalyst (40 mg), Na₂CO₃ (1 mmol), K₄[Fe(CN)₆] (0.2 mmol), DMF (4 mL) at 110 °C for 20 h.

The cyanation reaction of a variety of substituted haloarenes under the optimal condition (Table 3) was also examined. Both electron-donating / -withdrawing groups attached to the *para*- and *meta*-positions of bromoarenes produced the respective nitriles with good to excellent yields (Table 3, entries 1–9). Notably, 1,4-dibromobenzene was successfully converted to dicyanobenzene with 93% yield (Table 3, entry 10). The sterically hindered *ortho*-substituted and bulky substrates were also converted with ~82% yield of the corresponding nitriles (Table 3, entries 11–13). Further, catalytic runs of the less-active chloroarenes at 110 °C with longer reaction time produced nitriles with moderate yields (Table 3, entries 14–16). The prepared aryl nitriles were confirmed by NMR (Fig. S4-S27).

In order to check the heterogeneity of the Pd/TPA-TCIF catalyst, both hot filtration test and recycling experiment were conducted using 4-bromoanisole under the optimal conditions. In the hot filtration test (Fig. 7(a)), the catalyst was isolated by filtration after 8 h of reaction (with 48% of 4-methoxybenzotrile formation) under hot condition, and the filtrate was kept at 110 °C for the remaining reaction time (12 h). Upon termination of the reaction, no further increase in the yield of 4-methoxybenzotrile product was detected by GC. In addition, only a practically negligible amount of Pd (1.2 ppm) was detected in the filtrate by ICP-OES. In the recycling studies (Fig. 7(b)), the catalyst was recovered after the 1st run, washed with ethyl acetate and water, and dried under vacuum condition at 100 °C for 2 h before adding the recovered catalyst to a new reaction cycle. There was only a negligible drop in the activity for up to five successive cycles. After recycling, the catalyst was confirmed to retain its high crystallinity (Fig. 4), large BET surface area (2629 m² g⁻¹, Fig. 3(a)), and the deconvoluted Pd(II) binding energy peaks at 336.9 and 342.0 eV in Pd 3d XPS data (Fig. 6(a)). These results confirmed that the crystalline Pd/

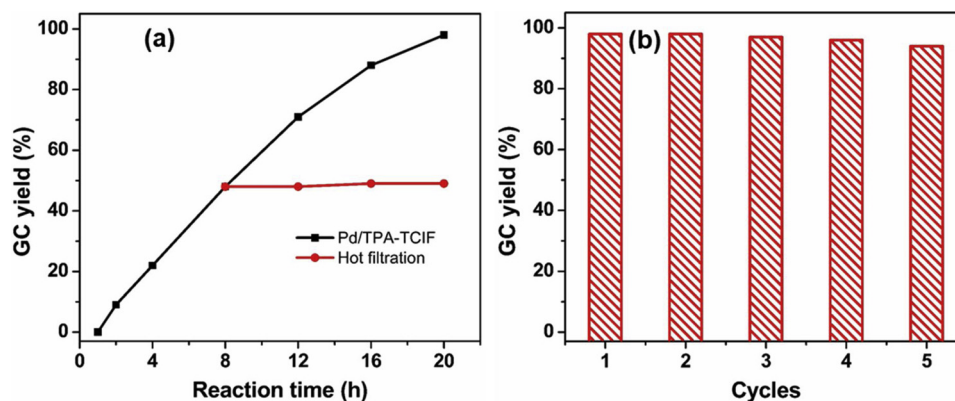


Fig. 7. (a) GC yield of 4-methoxybenzotrile as a function of reaction time and hot filtration test and (b) catalyst recycling studies for the cyanation of 4-bromoanisole over Pd/TPA-TCIF.

Table 3
Aromatic cyanation of haloarenes over Pd/TPA-TCIF.^a

Entry	Haloarenes	Product	GC yield (%)	TON
1	Bromobenzene	Benzonitrile	99	230
2	4-Bromoanisole	4-Methoxybenzotrile	98	228
3	4-Bromotoluene	4-Methylbenzotrile	95	221
4	4'-Bromoacetophenone	4'-Cyanoacetophenone	97	226
5	1-Bromo-4-nitrobenzene	4-Nitrobenzotrile	99	230
6	4-Bromobenzotrile	1,4-Dicyanobenzene	100	233
7	4-Bromobenzotrifluoride	4-(Trifluoromethyl)benzotrile	96	223
8	4-Bromobenzaldehyde	4-Formylbenzotrile	94	219
9	3-Bromotoluene	3-Methylbenzotrile	91	212
10 ^b	1,4-Dibromobenzene	1,4-Dicyanobenzene	93	216
11	2-Bromotoluene	2-Methylbenzotrile	84	195
12	2,4-dimethylbromobenzene	2,4-Dimethylbenzotrile	82	191
13	2-Bromonaphthalene	2-Cyanonaphthalene	86	200
14 ^c	Chlorobenzene	Benzonitrile	59	137
15 ^c	4-Chloroanisole	4-Methoxybenzotrile	64	149
16 ^c	4-Chlorotoluene	4-Methylbenzotrile	63	147

^a Haloarenes (1 mmol), Pd/TPA-TCIF (40 mg; 0.0043 mmol Pd), $K_4[Fe(CN)_6]$ (0.2 mmol), Na_2CO_3 (1 mmol), DMF (4 mL) 110 °C, 20 h.

^b $K_4[Fe(CN)_6]$ (0.4 mmol), catalyst (80 mg), Na_2CO_3 (2 mmol), 24 h; ^c36 h.

TPA-TCIF catalyst is robust and truly heterogeneous in nature.

Finally, the catalytic efficiency of Pd/TPA-TCIF for the cyanation of haloarenes in the presence of $K_4[Fe(CN)_6]$ was compared with those of several recently reported Pd-catalytic systems. Table S1 shows that Pd/TPA-TCIF is sufficiently active and competitive by considering its low catalyst loading, ligand-free reaction condition, moderate reaction temperature, and excellent recyclability.

4. Conclusions

A novel triazine-based covalent imine framework (TPA-TCIF) with a highly crystalline structure and excellent textural properties (surface area of $2938 \text{ m}^2 \text{ g}^{-1}$ and a pore volume of $1.32 \text{ cm}^3 \text{ g}^{-1}$) was synthesized by Schiff-base reaction of suitable monomers under solvothermal condition in butanol:dichlorobenzene solvent mixture. The product showed high chemical stability and was used as an effective carrier for anchoring Pd(II) ions via coordination interaction with the imine and/or triazine functionalities in TPA-TCIF. The prepared Pd/TPA-TCIF was used as a heterogeneous catalyst for the cyanation of bromoarenes in the presence of non-toxic $K_4[Fe(CN)_6]$ with excellent product yields. The inactive chloroarenes also proceeded to the corresponding cyanation products with moderate yields. Pd/TPA-TCIF was highly stable under the reaction conditions with no Pd(II) leaching or loss of activity after 5 successive cycles.

Acknowledgments

This research was supported by the Basic Science Research Program through the National Research Foundation of Korea (NRF) funded by the Ministry of Education (2015R1A4A1042434). PP acknowledges the support by the Korea Research Fellowship program funded by the Ministry of Science and ICT through the National Research Foundation of Korea (2017H1D3A1A02013620).

Appendix A. Supplementary data

Supplementary material related to this article can be found, in the online version, at doi:<https://doi.org/10.1016/j.mcat.2019.110395>.

References

- [1] S.-Y. Ding, W. Wang, *Chem. Soc. Rev.* 42 (2013) 548–568.
- [2] V.S. Vyas, M. Vishwakarma, I. Moudrakovski, F. Haese, G. Savasci, C. Ochsenfeld, J.P. Spatz, B.V. Lotsch, *Adv. Mater.* 28 (2016) 8749–8754.
- [3] M. Mu, Y. Wang, Y. Qin, X. Yan, Y. Li, L. Chen, *ACS Appl. Mater. Interfaces* 9 (2017) 22856–22863.
- [4] P. Puthiaraj, W.-S. Ahn, *Mol. Catal.* 437 (2017) 73–79.
- [5] X. Chen, W. Wang, H. Zhu, W. Yang, Y. Ding, *Mol. Catal.* 456 (2018) 49–56.
- [6] P. Puthiaraj, S.-M. Cho, Y.-R. Lee, W.-S. Ahn, *J. Mater. Chem. A* 3 (2015) 6792–6797.
- [7] S.-Y. Ding, M. Dong, Y.-W. Wang, Y.-T. Chen, H.-Z. Wang, C.-Y. Su, W. Wang, *J. Am. Chem. Soc.* 138 (2016) 3031–3037.
- [8] S. Ravi, P. Puthiaraj, K.H. Row, D.-W. Park, W.-S. Ahn, *Ind. Eng. Chem. Res.* 56 (2017) 10174–10182.
- [9] A.K. Mandal, J. Mahmood, J.-B. Baek, *ChemNanoMat* 3 (2017) 373–391.
- [10] P. Puthiaraj, K. Pitchumani, *Chem. Eur. J.* 20 (2014) 8761–8770.
- [11] J.-J. Kim, C.-R. Lim, B.M. Reddy, S.-E. Park, *Mol. Catal.* 451 (2018) 43–50.
- [12] K. Park, S. Lim, J.H. Baik, H. Kim, K.-D. Jung, S. Yoon, *Catal. Sci. Technol.* 8 (2018) 2894–2900.
- [13] F. Beuerle, B. Gole, *Angew. Chem. Int. Ed.* 57 (2018) 4850–4878.
- [14] N. Iranpoor, F. Panahi, F. Roozbin, S. Rahimi, M.G. Haghghi, *Mol. Catal.* 438 (2017) 214–223.
- [15] P. Puthiaraj, K. Pitchumani, *Green Chem.* 16 (2014) 4223–4233.
- [16] M.M. Trandafir, L. Pop, N.D. Hădăde, M. Florea, F. Neațu, C.M. Teodorescu, B. Duraki, J.A. van Bokhoven, I. Grosu, V.I. Părvulescu, H. Garcia, *Catal. Sci. Technol.* 6 (2016) 8344–8354.
- [17] P. Puthiaraj, Y.-R. Lee, S. Zhang, W.-S. Ahn, *J. Mater. Chem. A* 4 (2016) 16288–16311.
- [18] P. Puthiaraj, Y.-R. Lee, W.-S. Ahn, *Chem. Eng. J.* 319 (2017) 65–74.
- [19] X. Wang, Y. Zhao, L. Wei, C. Zhang, J.-X. Jiang, *J. Mater. Chem. A* 3 (2015) 21185–21193.
- [20] K. Dong, Q. Sun, X. Meng, F.-S. Xiao, *Catal. Sci. Technol.* 7 (2017) 1028–1039.
- [21] W. Zhang, L. Peng, C. Deng, Y. Zhang, H. Qian, *Mol. Catal.* 445 (2018) 170–178.
- [22] S.-Y. Ding, J. Gao, Q. Wang, Y. Zhang, W.-G. Song, C.-Y. Su, W. Wang, *J. Am. Chem. Soc.* 133 (2011) 19816–19822.
- [23] S. Lin, Y. Hou, X. Deng, H. Wang, S. Sun, X. Zhang, *RSC Adv.* 5 (2015) 41017–41024.
- [24] R.S.B. Gonçalves, A.B.V. de Oliveira, H.C. Sindra, B.S. Archanjo, M.E. Mendoza, L.S.A. Carneiro, C.D. Buarque, P.M. Esteves, *ChemCatChem* 8 (2016) 743–750.
- [25] W. Leng, Y. Peng, J. Zhang, H. Lu, X. Feng, R. Ge, B. Dong, B. Wang, X. Hu, Y. Gao, *Chem. Eur. J.* 22 (2016) 9087–9091.
- [26] W. Leng, R. Ge, B. Dong, C. Wang, Y. Gao, *RSC Adv.* 6 (2016) 37403–37406.
- [27] E. Verde-Sesto, E.M. Maya, Á.E. Lozano, J.G. de la Campa, F. Sánchez, M. Iglesias, *J.*

- Mater. Chem. 22 (2012) 24637–24643.
- [28] S. Roy, T. Chatterjee, B. Banerjee, N. Salam, A. Bhaumik, S.M. Islam, RSC Adv. 4 (2014) 46075–46083.
- [29] N. Salam, S.K. Kundu, R.A. Molla, P. Mondal, A. Bhaumik, S.M. Islam, RSC Adv. 4 (2014) 47593–47604.
- [30] Q. Sun, B. Aguila, J. Perman, N. Nguyen, S. Ma, J. Am. Chem. Soc. 138 (2016) 15790–15796.
- [31] A.V. Ushkov, V.V. Grushin, J. Am. Chem. Soc. 133 (2011) 10999–11005.
- [32] P. Anbarasan, T. Schareina, M. Beller, Chem. Soc. Rev. 40 (2011) 5049–5067.
- [33] K.W. Rosenmund, E. Struck, Ber. Dtsch. Chem. Ges. (A and B Series) 52 (1919) 1749–1756.
- [34] T. Sandmeyer, Ber. Dtsch. Chem. Ges. 17 (1884) 1633–1635.
- [35] M. Sundermeier, A. Zapf, M. Beller, J. Sans, Tetrahedron Lett. 42 (2001) 6707–6710.
- [36] S.K. Kristensen, E.Z. Eikeland, E. Taarning, A.T. Lindhardt, T. Skrydstrup, Chem. Sci. 8 (2017) 8094–8105.
- [37] D.T. Cohen, S.L. Buchwald, Org. Lett. 17 (2015) 202–205.
- [38] G.-Y. Zhang, J.-T. Yu, M.-L. Hu, J. Cheng, J. Org. Chem. 78 (2013) 2710–2714.
- [39] M. Sundermeier, S. Mutyala, A. Zapf, A. Spannenberg, M. Beller, J. Organomet. Chem. 684 (2003) 50–55.
- [40] T. Schareina, R. Jackstell, T. Schulz, A. Zapf, A. Cotté, M. Gotta, M. Beller, Adv. Synth. Catal. 351 (2009) 643–648.
- [41] T. Schareina, A. Zapf, M. Beller, Chem. Commun. (2004) 1388–1389.
- [42] Y. Ren, Z. Liu, S. He, S. Zhao, J. Wang, R. Niu, W. Yin, Org. Process Res. Dev. 13 (2009) 764–768.
- [43] P.Y. Yeung, C.M. So, C.P. Lau, F.Y. Kwong, Org. Lett. 13 (2011) 648–651.
- [44] R. Gerber, M. Oberholzer, C.M. Frech, Chem. Eur. J. 18 (2012) 2978–2986.
- [45] B. Mariampillai, J. Alliot, M. Li, M. Lautens, J. Am. Chem. Soc. 129 (2007) 15372–15379.
- [46] B. Karimi, M. Vafaezadeh, P.F. Akhavan, ChemCatChem 7 (2015) 2248–2254.
- [47] M. Gholinejad, A. Aminianfar, J. Mol. Catal. A: Chem. 397 (2015) 106–113.
- [48] B. Karimi, A. Zamani, F. Mansouri, RSC Adv. 4 (2014) 57639–57645.
- [49] A. Modak, J. Mondal, A. Bhaumik, Green Chem. 14 (2012) 2840–2855.
- [50] V. Polshettiwar, P. Hesemann, J.J.E. Moreau, Tetrahedron 63 (2007) 6784–6790.
- [51] M. Opanasenko, P. Štěpnička, J. Čejka, RSC Adv. 4 (2014) 65137–65162.
- [52] H. Yu, R.N. Richey, W.D. Miller, J. Xu, S.A. May, J. Org. Chem. 76 (2011) 665–668.
- [53] R. Gomes, P. Bhanja, A. Bhaumik, Chem. Commun. 51 (2015) 10050–10053.
- [54] W. Zhang, H. Huang, F. Li, K. Deng, X. Wang, J. Mater. Chem. A 2 (2014) 19084–19094.
- [55] L. Heymann, B. Schiller, H. Noei, A. Stierle, C. Klinke, ACS Omega 3 (2018) 3892–3900.
- [56] Z. Yang, M. Xu, Y. Liu, F. He, F. Gao, Y. Su, H. Wei, Y. Zhang, Nanoscale 6 (2014) 1890–1895.
- [57] M.J. Katz, Z.J. Brown, Y.J. Colón, P.W. Siu, K.A. Scheidt, R.Q. Snurr, J.T. Hupp, O.K. Farha, Chem. Commun. 49 (2013) 9449–9451.
- [58] S. Dey, A. Bhunia, D. Esquivel, C. Janiak, J. Mater. Chem. A 4 (2016) 6259–6263.
- [59] M. Matsumoto, R.R. Dasari, W. Ji, C.H. Feriante, T.C. Parker, S.R. Marder, W.R. Dichtel, J. Am. Chem. Soc. 139 (2017) 4999–5002.
- [60] C. Montoro, D. Rodríguez-San-Miguel, E. Polo, R. Escudero-Cid, M.L. Ruiz-González, J.A.R. Navarro, P. Ocoñ, F. Zamora, J. Am. Chem. Soc. 139 (2017) 10079–10086.
- [61] Q. Fang, S. Gu, J. Zheng, Z. Zhuang, S. Qiu, Y. Yan, Angew. Chem. Int. Ed. 53 (2014) 2878–2882.
- [62] Y. Zhi, P. Shao, X. Feng, H. Xia, Y. Zhang, Z. Shi, Y. Mu, X. Liu, J. Mater. Chem. A 6 (2018) 374–382.
- [63] X. Yu, Z. Yang, S. Guo, Z. Liu, H. Zhang, B. Yu, Y. Zhao, Z. Liu, Chem. Commun. 54 (2018) 7633–7636.
- [64] J. Zhang, L. Liu, H. Liu, M. Lin, S. Li, G. Ouyang, L. Chen, C.-Y. Su, J. Mater. Chem. A 3 (2015) 10990–10998.
- [65] N. Popp, T. Homburg, N. Stock, J. Senker, J. Mater. Chem. A 3 (2015) 18492–18504.
- [66] S. Mitra, H.S. Sasmal, T. Kundu, S. Kandambeth, K. Illath, D. Díaz Díaz, R. Banerjee, J. Am. Chem. Soc. 139 (2017) 4513–4520.
- [67] S. Mitra, S. Kandambeth, B.P. Biswal, A. Khayum M, C.K. Choudhury, M. Mehta, G. Kaur, S. Banerjee, A. Prabhune, S. Verma, S. Roy, U.K. Kharul, R. Banerjee, J. Am. Chem. Soc. 138 (2016) 2823–2828.
- [68] A.F.M. El-Mahdy, C.-H. Kuo, A. Alshehri, C. Young, Y. Yamauchi, J. Kim, S.-W. Kuo, J. Mater. Chem. A 6 (2018) 19532–19541.
- [69] S. Karak, S. Kandambeth, B.P. Biswal, H.S. Sasmal, S. Kumar, P. Pachfule, R. Banerjee, J. Am. Chem. Soc. 139 (2017) 1856–1862.
- [70] X. Yang, M. Zhen, G. Li, X. Liu, X. Wang, C. Shu, L. Jiang, C. Wang, J. Mater. Chem. A 1 (2013) 8105–8110.
- [71] C.M. Zinser, K.G. Warren, R.E. Meadows, F. Nahra, A.M. Al-Majid, A. Barakat, M.S. Islam, S.P. Nolan, C.S.J. Cazin, Green Chem. 20 (2018) 3246–3252.
- [72] B. Suresh Kumar, A.J. Amali, K. Pitchumani, ACS Appl. Mater. Interfaces 7 (2015) 22907–22917.